Responses of the tropical Pacific to wind forcing as observed by spaceborne sensors and simulated by an ocean general circulation model

W. Timothy Liu and Wenqing Tang

Jet Propulsion Laboratory

California Institute of Technology

Pasadena, CA 91109

Robert Atlas

Laboratory for Atmospheres

Goddard Space Flight Center

Greenbelt, MD 20771

accepted by J. Geophys. Res.

Abstract

in this study, satellite. observations, in situ measurements, and model simulations are combined to assess the oceanic response to surface wind forcing in the equatorial Pacific. The surface wind fields derived from observations by the.spat.ebornc Special Sensor Microwave Imager (SSMI) and from the operational products of the European Centre for Medium Range Weather Forecasts (ECMWF) are compared. When SSMI winds are used to form a primitive-equation ocean general circulation model (OGCM), they produce 3°C more. surface cooling than ECMWF winds for the eastern equatorial Pacific during the cool phase of an El Niño Southern Oscillation (ENSO) event. The stronger cooling by SSMI winds is in good agreement with measurements at the moored buoys and observations by the Advanced Very High Resolution Radiometer, indicating that SSMI winds are superior than ECMWF winds in forcing the. tropical ocean. in comparison with

1. Introduction

The combination of satellite observations and a numerical ocean circulation model has been promoted since the seventies as a potentially powerful tool to study the traditionally undersampled ocean, particularly to understand the basin-wide oceanic responses to atmospheric forcing. With the accumulation of data from operational sensors such as the Advanced Very High Resolution Radiometer (AVHRR) and the Special" Sensor Microwave Imager (SSh41), with the recent launching of research satellites such as Geosat, Topex/Poseidon, and ERS-1, and with the fast-improving accessibility of affordable supercomputer time to run the ocean general circulation model (OG

The equator-ial Pacific, where wind forcing is most directly felt and where the interannual signal caused by El Niño Southern Oscillation (ENSO) is large, is the selected region of this study. This region is also blessed with the Tropical Atmosphere and Ocean (TAO) buoy array and island tide gauges, all of which are part of the monitoring system of the Tropical Oceans and Global Atmosphere (TOGA) Program; the buoys and tide gauges provide

budget will be discussed in an attempt to shed light on the dominant mechanism by which surface. t emperat ure is changed by wind forcing. The conclusion is given in Section 7.

2. Ocean General Circulation Model

The Modular Ocean Model (MOM) developed at the Geophysical Fluid Dynamics Laboratory [Bryan and Cox, 197?] was used in this study. It is an improved and more general version of t he model used by Tang and Liu [1992]. The model uses Boussinesq and hydrostatic approximations. The vertical mixing coefficient is formulated as an empirical function of the Richardson number [Philander cl a].,] 987]. The horizontal domain is chosen to cover the Pacific Ocean from 30"S to 50°N and from 130°E to 70°W. Following the tradition for applying this model, a no-slip condition is applied at the lateral wall. Near the north and south boundaries, the temperature and salinity, are relaxed to the climatological seasonal values [Levitus, 1982], and no flux of heat or salt is allowed on the. east and west boundaries. The longitudinal resolution is 1° and the latitudinal resolution is]/3') within the equatorial band of 10° from the equator, but increases to 2.5" at north and south boundaries. The model has constant depth of 4149 m, with 27 levels. The model time step is one hour.

The initial conditions are the January climatological temperature and salinity, with no current. The

The OGCM was run for a 3.5-year period, driven by climatological wind stress [Hellerman ant] Rosenstein, 1983]. A fter this 3.5-years spin-up, the model reaches a quasi-equilibrium seasonal cycle, '1 'hen three parallel runs were started by applying two different wind stress fields (as discussed in Section 3) and by continuing the run with climatological forcing as the control, covering three years, starting July 1987.

ave.raged over the model domain is equal to zero at each inversion step. The sea level is then computed from the hydrostatic relation

$$P = \rho g H$$

where ρ is the surface density and g is the acceleration due to gravity.

3. Data

Three sets of wind fields are used to force the model. The first set consists of the m'ind-stress fields computed by 1 lellerman and Rosenstein [1 983] from 1 16 years (1 870-1986) of wind reports from volunteer ships, using Bunker's [1 976] drag coefficients, which increase with wind speed and atmospheric instability. This wind climatology is used in spinning up the model and as a control run. The second set consists of wind velocity field at 10-m height, taken from the ECMWF/TOGA (Tropical Oceans and Global Atmosphere) Level 1 II data set. This is the non-initialized, analyzed data field produced by the NWP center at the I ECMWF [Bengtsson et al., 1982]. This set of data is, hereafter, referred as "ECMWI winds". 'I 'he. third set is based on wind speed measured by the SSM1 [Wentz 1992]. The wind direction is determined by a variational method using all available data [Atlas et al., 1991, 1993]. This set of data is, hereafter, referred to as "SSh41 wind s". Three years of data, from July 1987 to June 1990, from the. latter two data sets are used in this study

In computing wind stress from ECMWF and SSMI winds, a variable drag coefficient that accounts for the transition from rough flow (high wind) to smooth flow (low wind) and for variation in the

1000 mb derived from the initialized analysis, and this product was used by Busalacchi et al. [1993] to compare with the first year of SSMI winds. The uncertainty in the altitude of the isobaric surface, however, poses a serious problem for converting the wind vector into momentum flux, or wind stress, because the wind shear near the surface could be large. The ECMWF/TOGA Level 111 archive was produced partly to alleviate this difficulty. The climatological wind is monthly at a 2° latitude by 2° longitude spatial resolution. The SSMI wind has a 6-hourly and 2° latitude by 2.5° longitude resolutions while the ECMWF wind has a semi-daily and 2.5° by 2.5° resolutions. The wind data are linearly interpolated to the time step (hourly) and to the spatial grid of the OGCM.

The SST is taken from 1° latitude by 1 c. longitude. and weekly maps produced through optimal interpolation using AVHRR data blended with in situ data [Reynolds and Smith, 1994] and this data set is, hereafter, referred to as the "AVHRR SST". Sea level residues from the Geosat altimeter start from the geophysical data records with environmental corrections [Cheney et al., 1987]. Subsequent processing, including

The means and variances of the SSMI and ECMWF winds for the three-year period have similar geographical distributions but different strc)lp.tits, To find out the statistical significance of the differences between the means and the variances, standard Student's t and F tests are performed [Press et al., 1989]. Large and significant differences of the mean are found between 25°N and 25°S in the Pacific Ocean, excepted in an area roughly within 200 km from the American coast north of the 10°N, in an area west of 170°E between the equator and 10°S, and in a narrow zonal belt along the equator between 80°W and 120°W. The mean differences are. large along two zonal belts centered at 15°N and SC'S, We have no good explanation on the distribution. Large and significant values of F are found in the eastern and western Pacific within 20° latitude north of the equator.

While the underlying cause for the distributions of the normalized mean difference. and ratio of variance is not apparent, the temporal characteristics of the. differences are revealed in time series comparisons at selected off-equatorial locations in Fig. 2 and equatorial locations in Fig. 3. The 12hourly data are passed through a 1 ()-day running mean filter to give. graphic clarity in the figures. In 1 ig. 2, the temporal variations are dominated by periods of strong wind separated by quiescence periods of low wind. The strong winds are easterly, except at 5°N and 80°W. The two sets of wind appear to roughly agree during the quiescence periods, but SSMI winds indicate much more strength at the peak of the strong wind events. Unfortunately, there is no high quality in situ wind measurements to evaluate the two sets of winds at these off-equatorial locations where the differences are relatively large

There are in situ wind measurements from the TAO moored buoys along the equator, but the. mean difference between SSMI and ECMWF winds are relatively small at these locations. The buoy measurements and the climatological annual cycles are

included in Fig 3. The difference in intensity during wind events can are still present. At 1 65°E, buoy measurements at latitudes 2°N, 0°, and 2°S arc averaged together because there arc. large data gaps at each latitude, but for the other three longitudes, only measurements at the equator are used. The climatological annual cycles shown in the figure arc compiled from buoy data; the length of the data sets varies from approximately 6 years at 170C'W to 11 years at 1400W. The annual cycle is prominent at] 1 O°W and 140°W, but bc.comes less conspicuous at 170°W and 165"1 ;. Both SSMI and ECMWF winds show eastward anomalies during the. warm phase of ENSO in 1987 at all three stations cast of the elate-line and westward anomalies during the cold phase of ENSO in 1988 at 165°E and 170°W.

Using three years SSMI and ECMWF data coincident with the daily buoy

To clarify the. difference in temperature response to SSMI and ECMWF wind forcing], time series of the first- level (5-1])) temperature produced by the OGCM when forced by various winds are compared with the AVHRR SST and measurements made at equatorial buoys (Fig. 4). Sufficiently continuous SST measurements are available only at three equatorial moorings (110°W, 140°W, and 165 °E). The climatological annual cycle is compiled from seven years (July 1983 to June 1990) of the AVHRR SST. For all four location s, the model starts at temperatures that resulted from climatological winds and are close to climatological SST, which is lower than the. observations at locations east of the.elate-line. When more realistic winds from the ECMWF and SSMI are applied, the model temperature adjusts to observed values at locations after a few months and remains in rough agreement with observations extending through the warm phase of ENSO. Starting in March 1988, the observed temperature dropped sharply to below climatological values; the drop is more than 7°C at 11 0°W. The warm and cold ocean temperature anomalies during the 198"/--- 1988 ENSO event have been described by McPhaden and 1 layes [1990] and others, using, data from TAO buoys. When the model is forced by SSMI winds, the model temperature drops by an amount similar to the observed temperature drops (from AVHRR and buoy data), but the model temperature resulting from ECMWF wind forcing remains at climatological values at locations east of the date line. The difference in temperatures caused by ECMWF and SSMI forcing exceeds 3°C in October 1988 at all three locations east of the date line. Similar differences in SST simulations were observed by Tang and Liu [1992].

East of the. date-line, the temperatures start to rise around November 1988 and approaches climatological value in early 1989, but the model temperatures that result from ECMWF winds are always higher than those resulting from SSMI winds. For 1990 at the. stations east of the date. line, both model simulations indicate cold anomalies not

present in the observations. At 165°E, the differences between model simulations relatively small and there are general agreement between the model simulation and the observations, except during, the periods June—1 December 1989 and May-June 1990; the mason for these discrepancies is unclear.

The maximum differences in mean zonal wind stress are off the equator and the coast, as shown in Fig. 1, but the largest differences in SST response (not shown) are bounded to the eastern equatorial Pacific and the American coast. At the three locations east of the date-line., the SST simulations forced by ECMWF winds have significantly larger deviations from observations by AVHRR than simulations forced by SSMI winds, in both mean and variance, as shown in Table 1. Similarly, using, SSMI wind also significantly improve the correlation coefficient between SST simulations and observations. The statistics in Table 2 are computed from 363 pairs of data in 3 year at 3 day resolution. The probabilities that the reduction in mean and variance of the "errors" (deviation from observations) arises by pure chance from "errors" distributions with equal means and variances are less than 1 % for all locations, except the 10% value for variance at 110°W. The probability that the improvement of correlation by SSMI winds arises by pure chance from two distributions with equal correlations are less than 1 % at 140°W and 130°W, and increases only to 3% at 110°W. Similar conclusion can be drawn with buoy surface, temperature replacing AVHRR data.

The close agreement between AVHRR and buoy SST is an indication of the high quality of observations. The most striking result shown in Fig. 4 is that the SSMI wind produces a more realistic anomalous surface cooling in 1988 for the cool phase of ENSO than ECMWF wind does. Another implication is on the robustness of the OGCM. All the correlation coefficients between models simulations and observations are significant; there are less than 1 % chance that the correlation are results of chance. Overall, the

model simulates the temporal variability of SS"1' when forced by winds with reasonable realistic temporal signal. There are periods when model simulations are. different from observations under both wind forcing; the differences are likely to be caused by the deficiency of model physics or the lack of realistic thermal and hydrologic forcing

5.2. **Steric Level**

The temperature difference should be reflected in density structure and the wind forced temperature response is not likely be confined to the surface. The depth integrated density response to different wind forcing is examined in Fig. 5, where the variation of steric level (dynamic height) between 300 m and the surface at the four buoy locations is shown. The temporal

For 1987, the buoy data are more

5.3. Sea Level

reflecting the transition from the warm to the cool phases of 1 ENSO. However, no such trend is found in Geosat data; the sate.]lilc dat a show a higher sea level than other data for the cool phase of ENSO in the boreal summer and fall of 1988. Unfortunately, there. is no altimeter data after February 1989. and the altimeter sampling is quite different from the other three data sets,

In general, the. sea level change derived from OGCM and the sea level from the altimeter agree with the tide gauge, as suggested by previous evaluations of Geosat altimeter data in the tropical Pacific using in situ measurements [Cheney et al., 1989; Wyrtki and Mitchum, 1 990; Tai et al., 1 989] and simulated dynamic height [Chao et al., 1 993]. The correlation coefficients between model simulations and observations at tidegauges shown in Table 3 are all significant with less than 1% probability that the correlation coefficients arise by pure chance from uncorrelated data. Although the model responses to the SSMI winds have higher correlation with tide gauge data than the responses to the ECMWF winds, the improvement in correlation are small. The differences in correlation coefficients are. obviously insignificant at Nauru and Kanton and there are slightly less than 20% probability that the improvements at other stations arise by chance.

S.4. Zonal Current

A comparison of zonal currents at 1 0-m depth and 1(0] n depth is presented in Fig. 7 for three locations where in situ current measurements are available. Since the buoy data include strong big)]- frequency variations, a 10-day running mean filter has been applied for clearer display. At both levels, the OGCM results from both wind forcing do not agree very well with the results derived from buoy data. The correlation coefficients between current simulations and observations are largely insignificant. The

low correlation between mode.1

Under both wind forcing, the sum of the first four terms cm the right side of the equation (not shown) agree very closely with the term of the left, both in magnitude and in variation, suggesting that the diffusion transport D is negligible. The variations of T averaged over this volume (not shown) are similar to the variations of SST. In Fig. 9, the difference between the two wind forcing is clearly evident in the difference in $\partial T/\partial t$ during March and May, 1988. With both wind forcing, the surface heat flux and all advection components contribute to the change of heat storage, but the largest terms are the warming by the surface heat flux and the cooling due to vertical advection; they largely compensate each other. 1)uring the onset of the 1988 cold phase, SSMI winds forced a higher thermocline and facilitated vertical heat transport by upwelling.

7. Discussion and Conclusion

The results of this study contribute in three areas. They show that spacebased winds are superior than NWP winds in forcing realistic oceanic response, infer some deficiencies

integrated ef fect of different winds. ‘1 ‘he steric chang es shoul d fo] I ow

The inference is that mixed layer depth and vertical advection are the dominant wind driven factors for anomalous SST changes. Significant differences in zonal wind stress are found off-equator while significant differences in temperature are more confined to the equator and coastal regions, demonstrating that

'l'his study was performed at the Jet Propulsion Laboratory, California institute of 'J'ethnology, under contract with the National Aeronautics and Space Administration (NASA). The SSMI wind field was produced at the NASA Goddard Space Flight Center. We arc! grateful to Victor Zlotnicki for his version of the Geosat sea level. This study was supported by the NASA Scatterometer Project, the Topex/Poseidon Project, and the Earth Observing System Interdisciplinary Science Investigation.

References

Atlas, R., S.C. Bloom, R.N. Hoffman, J. Ardizzone, and G. Brin, Space-based surface wind vectors to aid understanding of air-sea interactions, *EOS Trans. Amer. Geophy. Union, 72,* 201-208, 1991.

Atlas, R., R.N. Hoffman, and S.C. Bloom, Surface wind velocity over the ocean. *Atlas of Satellite Observations Related to Global Changes*, R.J. Gurney, J. 1.. Foster, and C.L. Parkinson (eds.), Cambridge Univ. Press, London, 12.9-139, 1993.

Bengtsson, 1.., M. Kanamitsu, P. Kallberg, and S. Uppala, FGGE 4-dimensional data assimilation] at ECMWF, *Bull. Am. Meteorol. Soc., 63,* ?9-43. 1982.

Bryan, K., and M.I D. Cox, An approximate equation of state for numerical models of ocean circulation, *J. Phys. Oceanogr., 2*, 510-514, 19'?2.

Bunker, A.F., computations of surface energy flux anti annual air-sea interaction cycles of the North Atlantic Ocean, *Mon. Wea. Rev., 104*, 1122-1140, 1976.

Busalacchi, A .J., R.h4. Atlas, E.C.) Jackert, Comparison of special sensor microwave imager vector wind stress with model-derived and subjective products for the tropical Pacific, *J. Geophys. Res.*, 98.6961-6977, 1 993.

Chao, Y., D. Halpern, and C. Perigaud, Sea surface height variability during 1986-1988 in the, tropical Pacific Ocean, .1. *Geophys. Res., 98*, 6947-6959, 1993.

Cheney, R.E., B.C. Douglas, R.W. Agreen, L. Miller, and D.L. Porter, *Geosat Altimeter Geophysical Data Record User Handbook*, NOAA Tech. Memo. NOS **NGS-46,** Natl. Geod. Surv., Rockville, MD, 20pp., 1987.

Cheney, R.E., B.C. Douglas, and L. Miller, Evaluation of' Geosat altimeter data with application to tropical Pacific sea level variability, *J. Geophys. Res.*, **94, 4737-4747, 1989.**

Enfield, D.B., Zonal and seasonal variation of the. Ile.ar-surface heat balance of the equatorial Pacific Ocean, *J. Phys. Oceanogr.*, 16, **1038-1054,** 1986.

Gill, A.E., and P.P. Niiler, The theory of the seasonal variability in the ocean, *Deep-Sea Res.*, 20, 141-177, 1973.

Halpern, D.,

general circulation model and reference to observations, *J. Geophys. Res. 100*, 2515-2522, 1995.

Hayes, S.P., L.J. Mangum, J. Picaut, A. Sumi, and K. Takeuchi, TOGA-TAO: A moored

Liu, W.T., W. Tang, and 1,.1,. Fu, 1995: Recent warming event in the Pacific may be an El Niño. *Eos Trans. Amer. Geophys. Union,* 43,429 and 437.

McPhaden, M.J., and S. Hayes, Variability in the eastern equatorial Pacific Ocean during 1986-1988, *J. Geophys. I< es., 95, 1319.5-13208,*] 990.

Oort, A.]]., Y.H. Pan, R. W. Reynolds, and C.F. Ropelewski, Historical trends in the surface temperature over the oceans based on the COADS, *Climate Dyn.,* 2, 29-38, 1987.

Philander, S.G.H., W.J. Hurlin and A.D. Seigel, A mode] of the seasonal cycle in the tropical Pacific Ocean, *J. Phys. Oceanogr., 17,* 1986-2002, 1987.

Press, W.}]., B.P. Flannery, S.A. Teukolsky, W.T. Vetterling,

Wyrtki, K., K. Constantine, B. Kilonsky, G. Mitchum, B. Miyamoto, T. Murphy, and S. Nakahar, *The Pacific Island Sea Level Network*, JIMAR Data Rep. 002, Univ. of Hawaii, Honolulu, 71pp. 1988.

Wyrtki, K. and G. Mitchum, Interannual difference of Geosat altimeter heights and sea level: the importance of a datum, *J. Geophys. Res., 95,* 2969-2975, 1990.

Zlotnicki, V., L.L. Fu, and W. Patzert, Seasonal variability in global sea level observed with Geosat altimetry, *J. Geophys. Res., 94*, 17959-17969, 1989.

Table] : Evaluation of OGCM simulations of surface temperature (°C) forced by SSMI

SSMI

ECMWF

Significance

"l'able 2: Same as *'l-able* 2, except for dynamic height (m) instead of surface temperature and buoy data instead of AVI 1 RR.

	Mean of Deviation from Buoy Data	Variance	Correlation Coefficient
	140°\17		
SSMI	0.067	0.00:31	0.71
ECMWF	0.102	0.0033	0.71
Significance	0.000	0.694	0.960
	110°W		
SSMI	0.081	0.0039	0.54
ECMWF	**0.142**	**0.()()40**	**(1.46**
Significance	0.000	0.681	0.185

Table 3: Correlation Coefficients between simulate.c] sea level change and Tidegauge observations. The probability that the difference in the coefficients arises by chance from equal values are listed under Significance .

Statio ------ _ _____	SSMI	ECMWF	Significance.
Rabaul	0.83	0.79	0.16
Kapingamarangi	0.78	0."/5	().29
Nauru	0.63	0,0?	0.96
Kant on	*0.67*	0.66	0.84
Christmas	0.71	0.66	().1"/
Santa Cruz	0.61	054	*0.19*

Figure Legends

Fig. 1 Distribution of the absolute value Student's t which is the mean difference between SSMI and ECMWF zonal wind stresses divided by the standard error (upper) and F function which is the ratio of the variances of the two zonal wind stresses (lower). Areas where the values of Student's t and F function has more than 1 % probability to come by pure chance from wind stresses of equal means and varainces are stippled.

Fig. 2 Comparison of the zonal component of surface wind stress derived from SSMI observations and from ECMWF analysis at selected locations (latitudes and longitudes are indicated in the figure).

Fig. 3 Same as [2], but at 4 selected locations along the equator and with additional comparison with buoy measurements

Fig. 4 Comparison of first-level (5-m) temperatures produced by the OGCM, when forced by SSMI and ECMWF winds, with AVHRR and buoy SST at four locations (longitudes are indicated in the figure) along the equator. The climatological annual cycle derived from the AVHRR SST is also shown.

Fig. 6. Comparison of sea level change derived from the OGCM, when forced by SSMI and ECMWF winds, with measurements at tide gauge stations (locations are indicated in the figures) and observations by the Geosat altimeter.

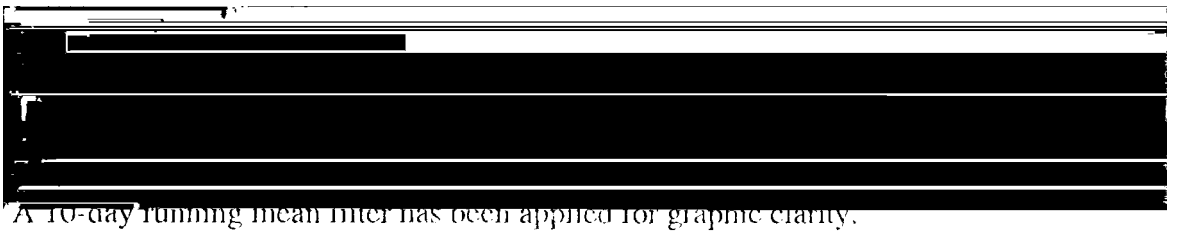

A 10-day running mean filter has been applied for graphic clarity.

Fig. 8. Time—depth variation of temperature from the model driven by SSMI winds (left) and the time---depth variation of the difference between temperatures from the OGCM drive.11 by SSMI and ECMWF winds (right).

Fig. 9. Ocean heat budget componen

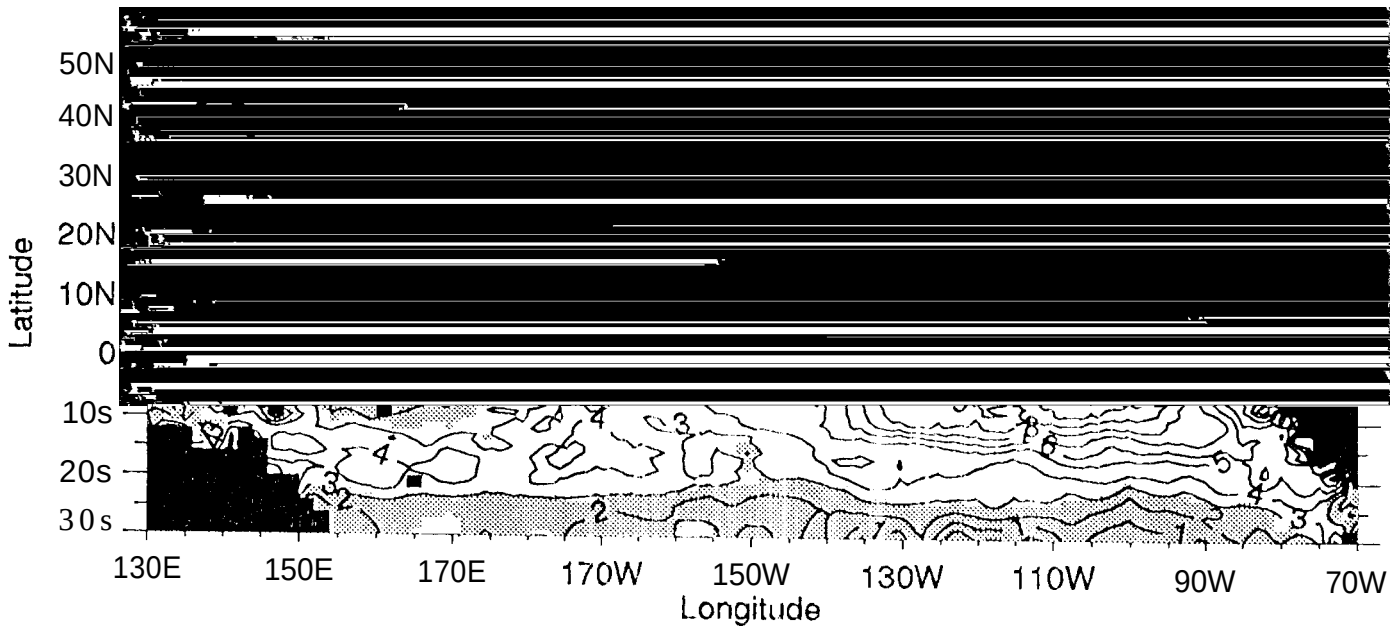

F-test for Significantly Different Variance

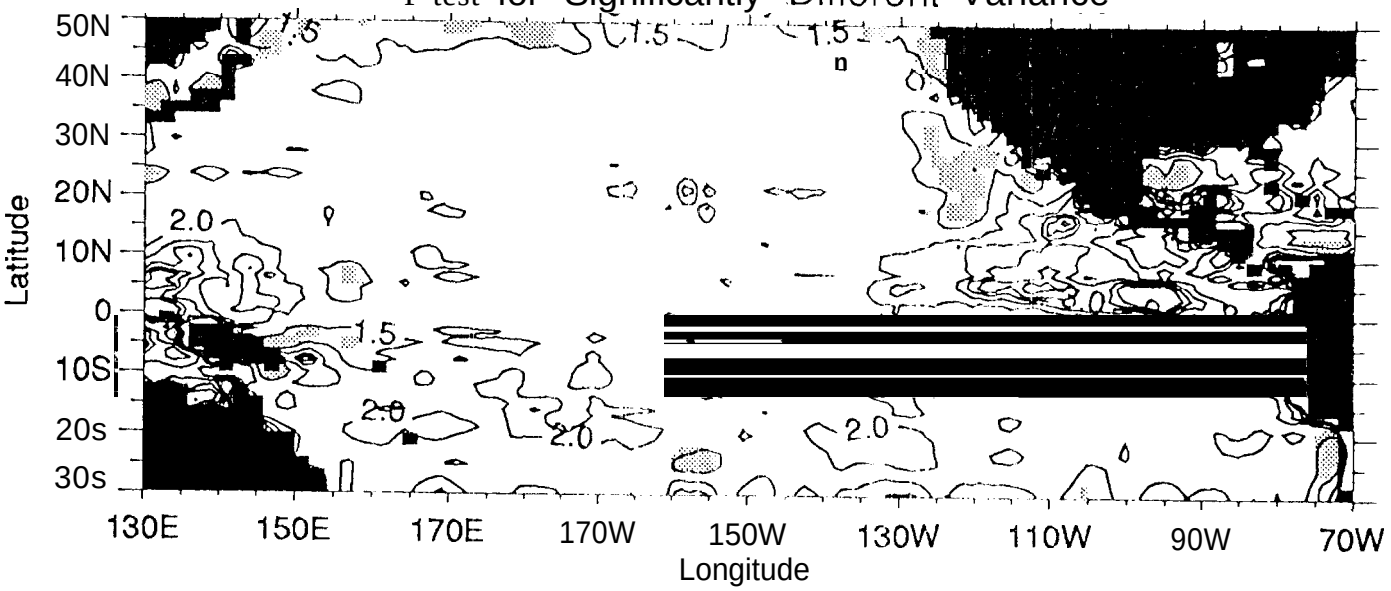

Plotted Mar 81996

Sea Surface Zonal Wind Stress

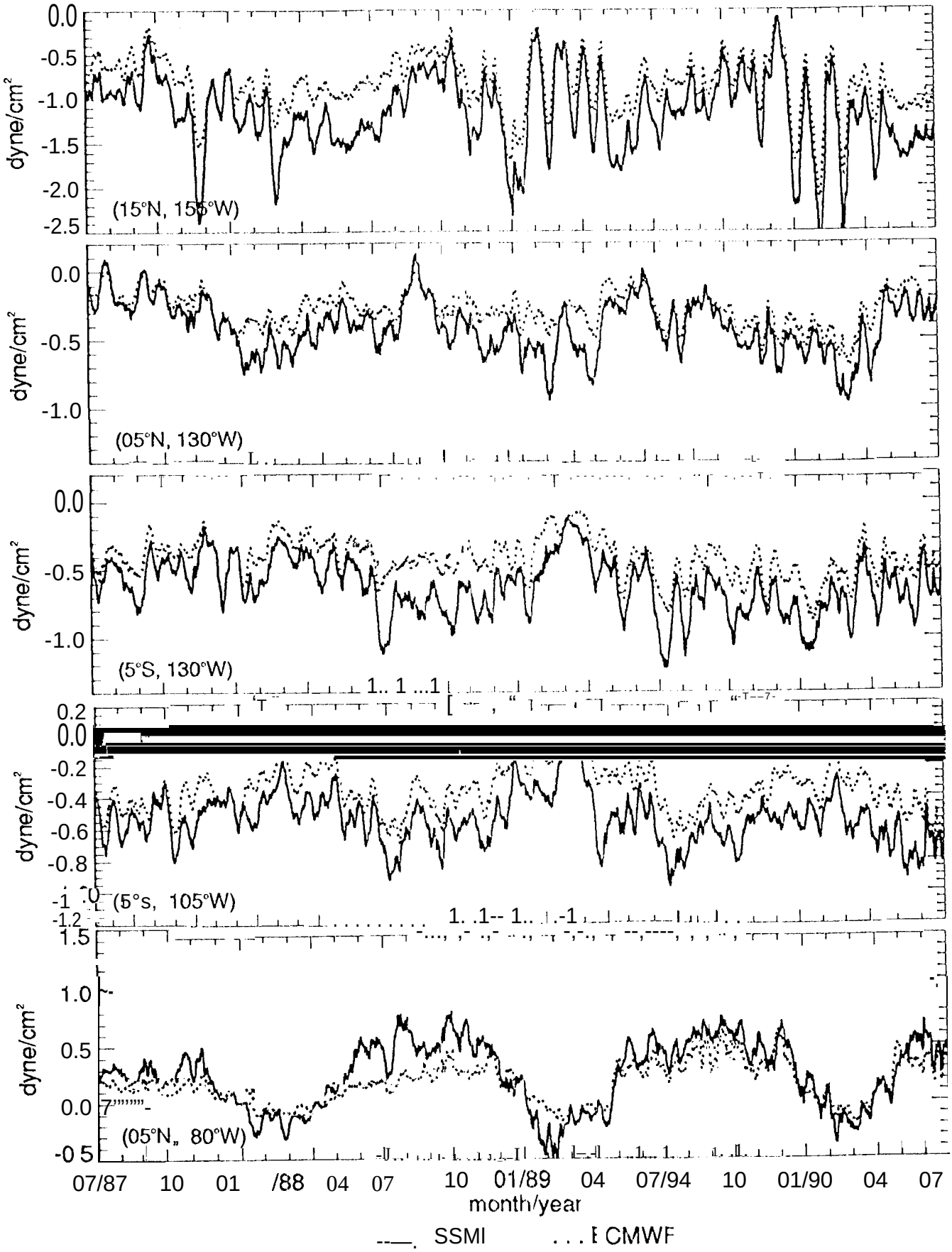

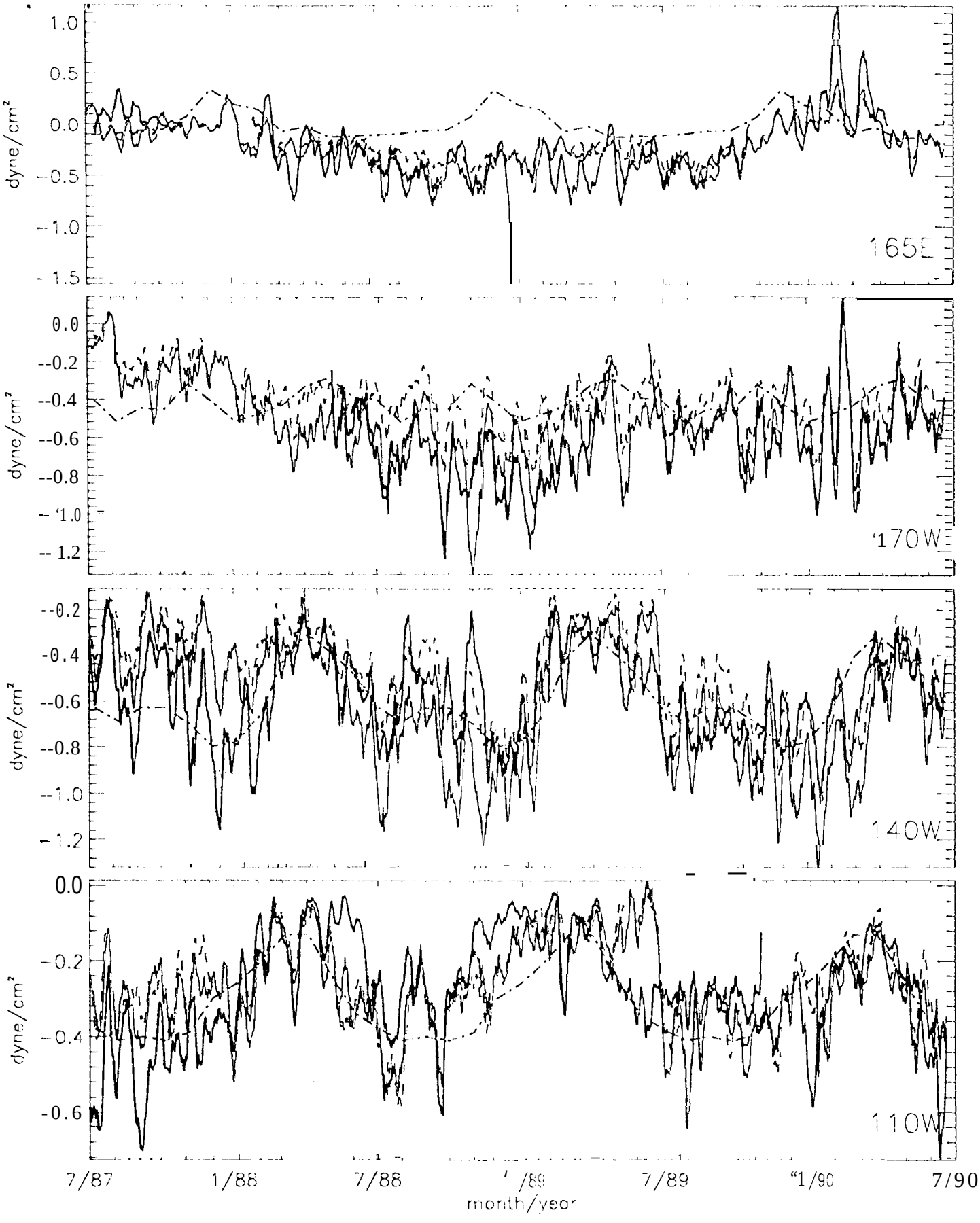
1.0
0.5
0.0
-0.5
-1.0
-1.5
dyne/cm²
165E
0.0
-0.2
-0.4
-0.6
-0.8
-1.0
-1.2
dyne/cm²
170W
-0.2
-0.4
-0.6
-0.8
-1.0
-1.2
dyne/cm²
140W
0.0
-0.2
-0.4
-0.6
dyne/cm²
110W
7/87
1/88
7/88
/89
7/89
1/90
7/90
month/year
Buoy
SSM
ECMWF
climatology

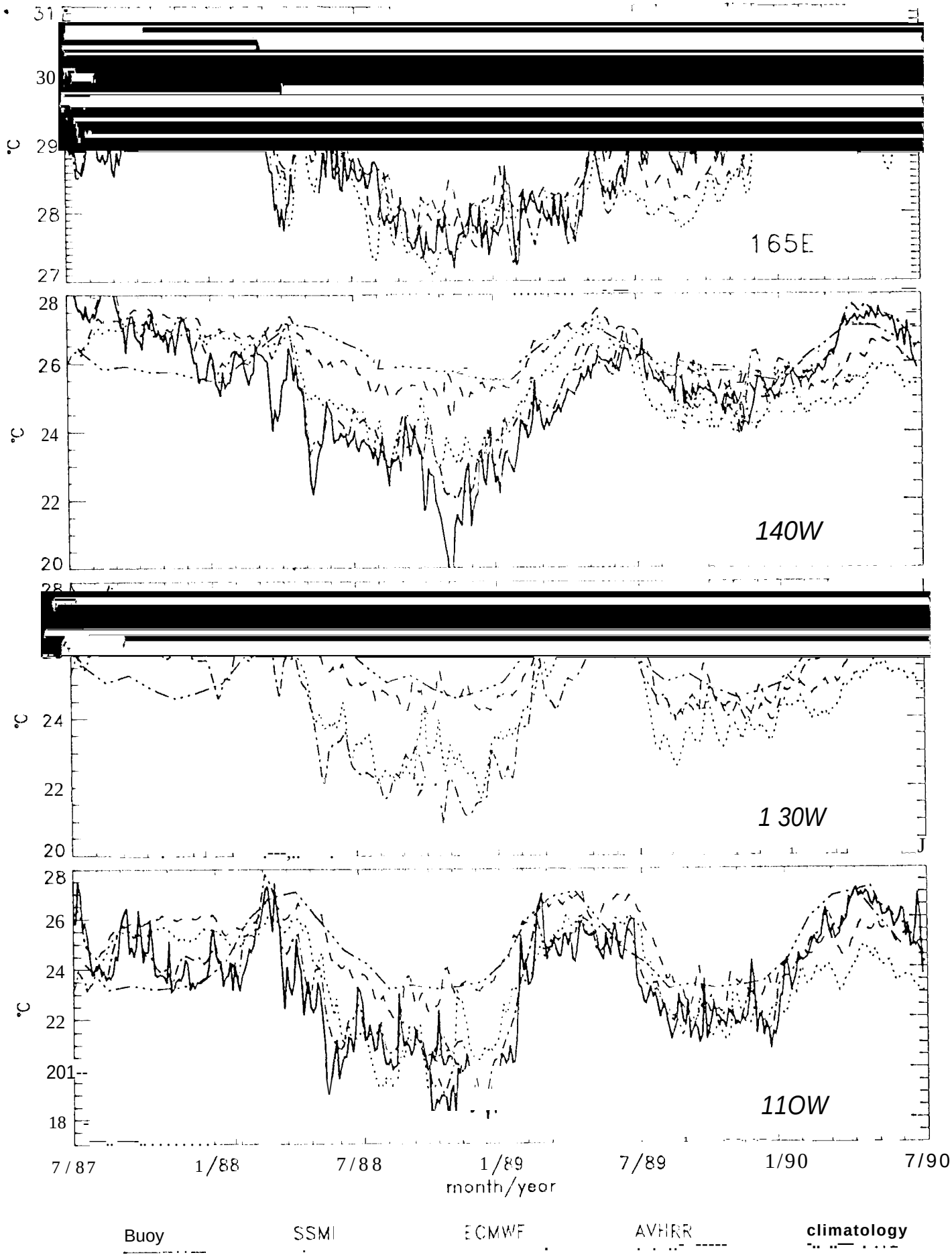
165E
140W
1 30W
11OW
°C
7/87
1/88
7/88
1/89
7/89
1/90
7/90
month/yeor
Buoy
SSMI
ECMWF
AVHRR
climatology

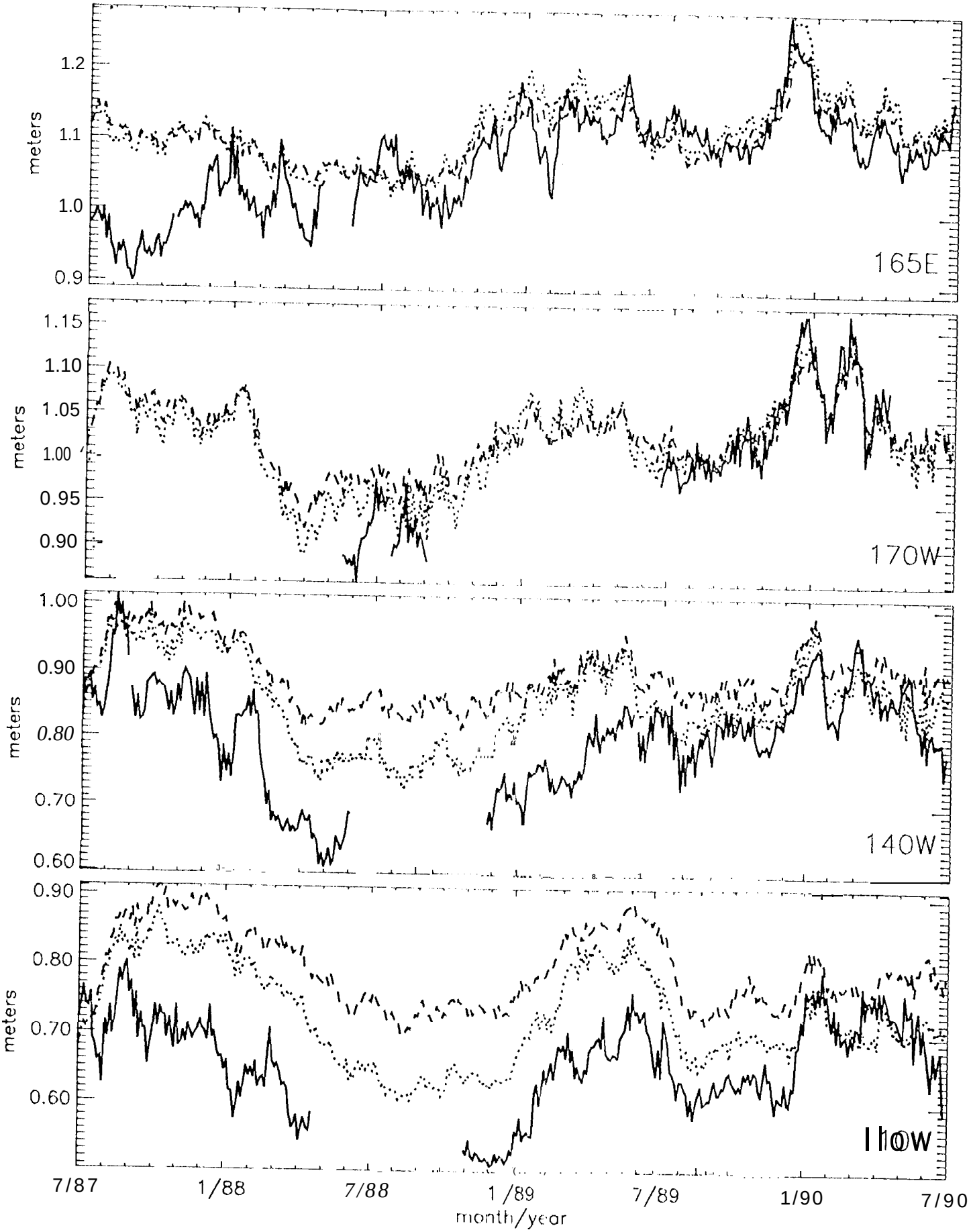
meters
1.2
1.1
1.0
0.9
165E
meters
1.15
1.10
1.05
1.00
0.95
0.90
170W
meters
1.00
0.90
0.80
0.70
0.60
140W
meters
0.90
0.80
0.70
0.60
110W
7/87
1/88
7/88
1/89
7/89
1/90
7/90
month/year
Buoy
SSMI
ECMWF

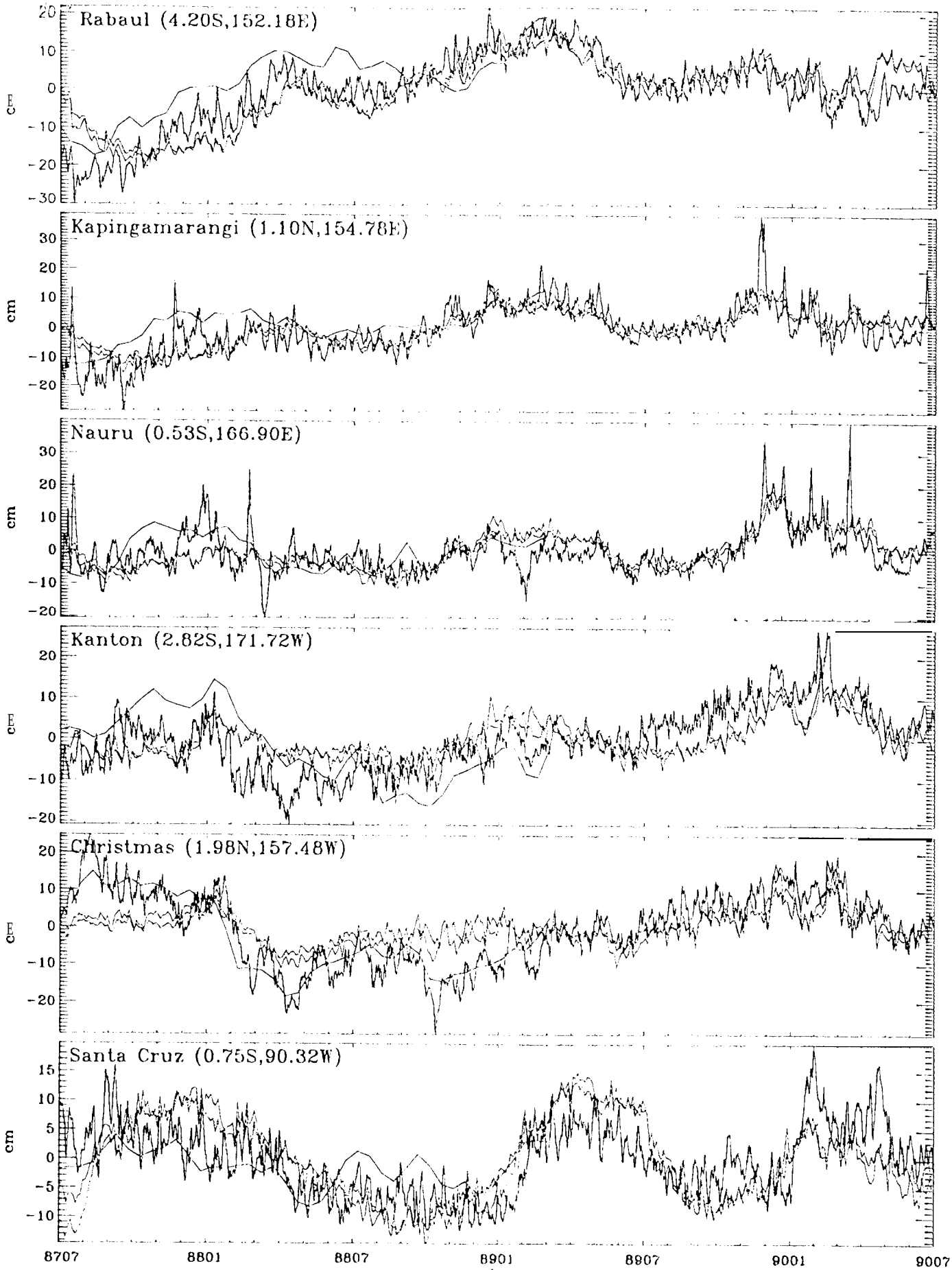
Rabaul (4.20S,152.18E)
Kapingamarangi (1.10N,154.78E)
Nauru (0.53S,166.90E)
Kanton (2.82S,171.72W)
Christmas (1.98N,157.48W)
Santa Cruz (0.75S,90.32W)
cm
8707
8801
8807
8901
8907
9001
9007
year/month
T-Tidegage
S-SSMI
E-ECMWF
G-Geosat

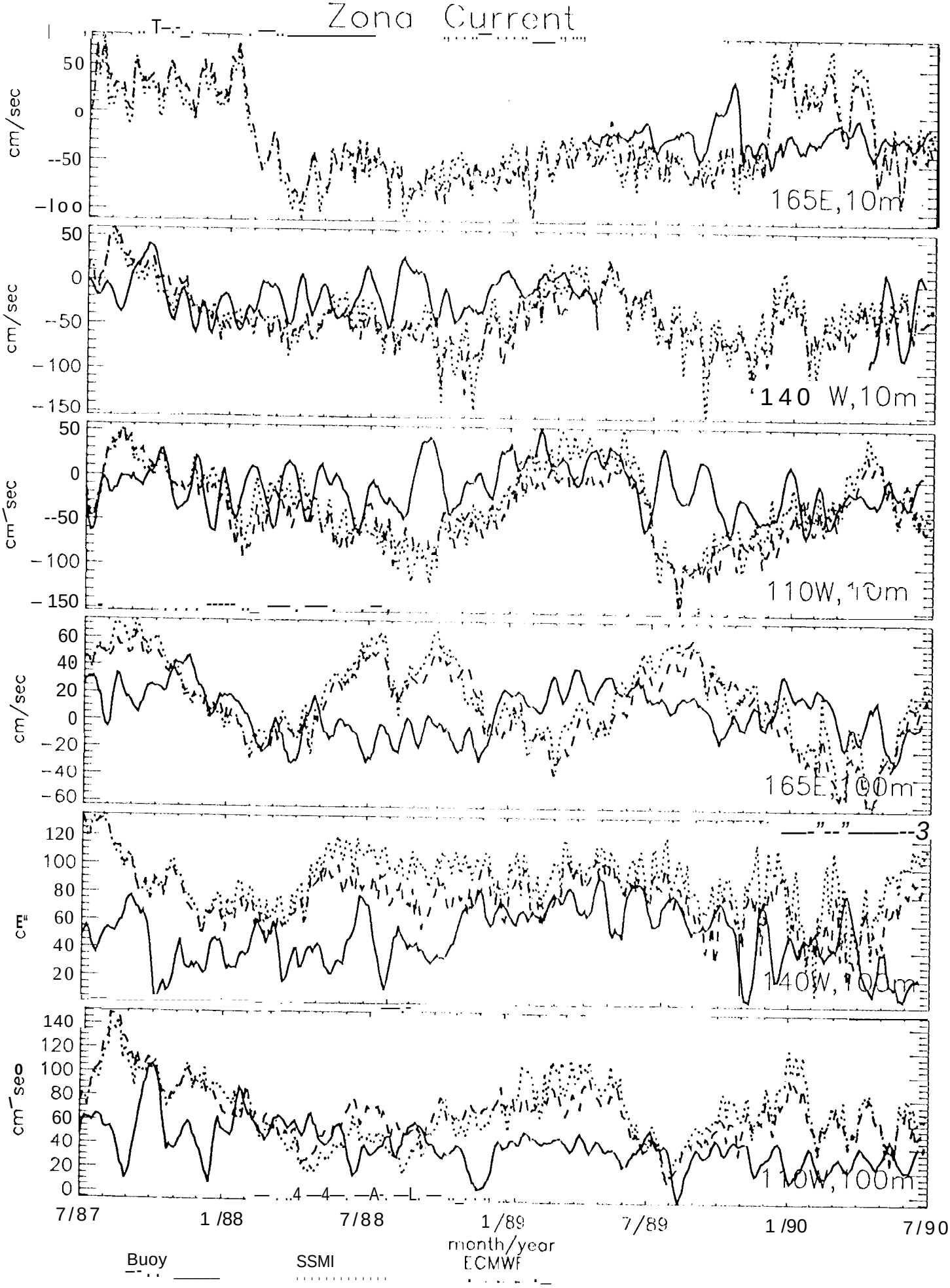
Zona Current
cm/sec
50
0
--50
−100
165E,10m
cm/sec
50
0
−50
−100
−150
140 W,10m
cm/sec
50
0
--50
−100
−150
110W,10m
cm/sec
60
40
20
0
−20
−40
−60
165E,100m
120
100
80
60
40
20
140W,100m
140
120
100
80
60
40
20
0
110W,100m
7/87
1/88
7/88
1/89
7/89
1/90
7/90
month/year
Buoy
SSMI
ECMWF

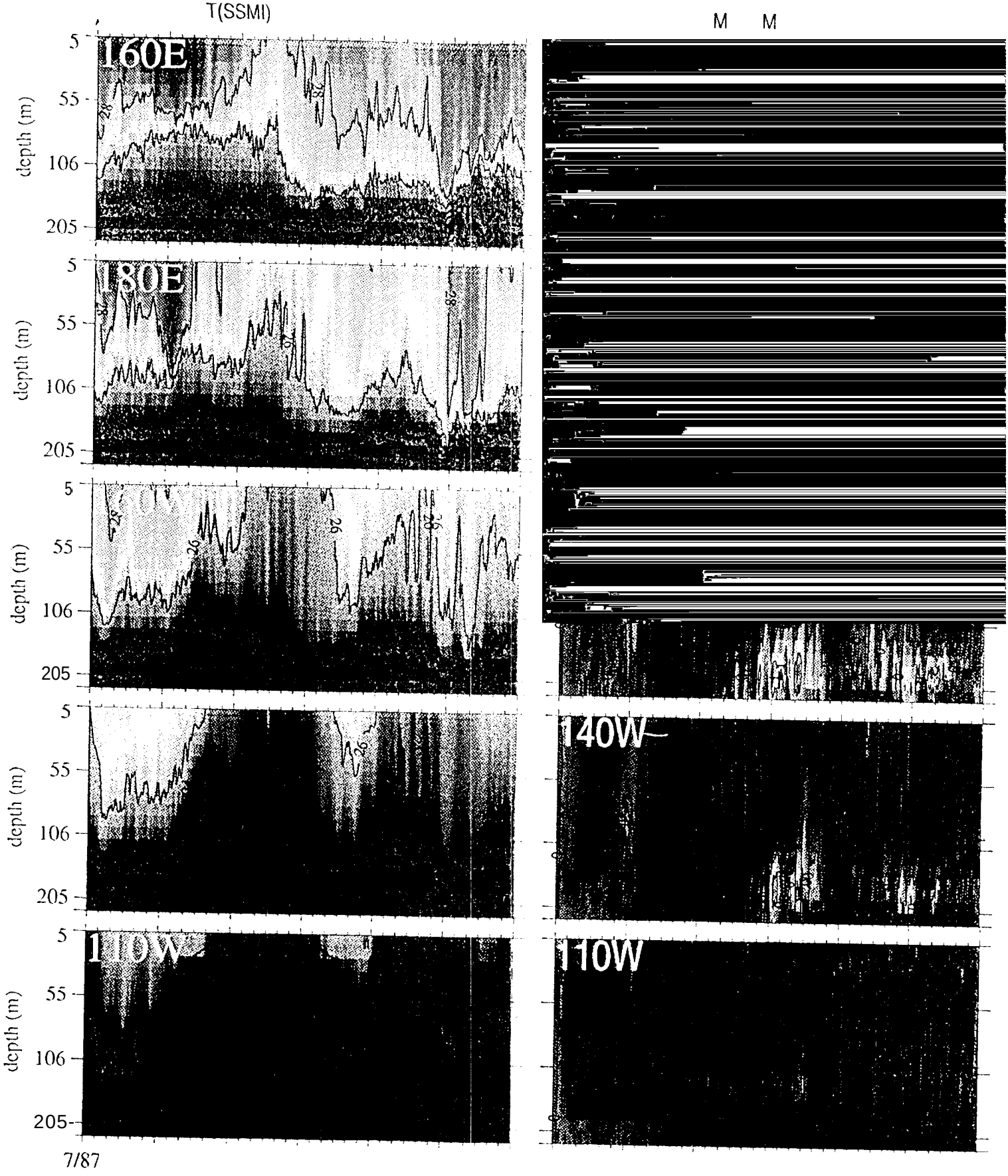
T(SSMI)
M M
160E
180E
140W
110W
110W
depth (m)
5
55
106
205
7/87

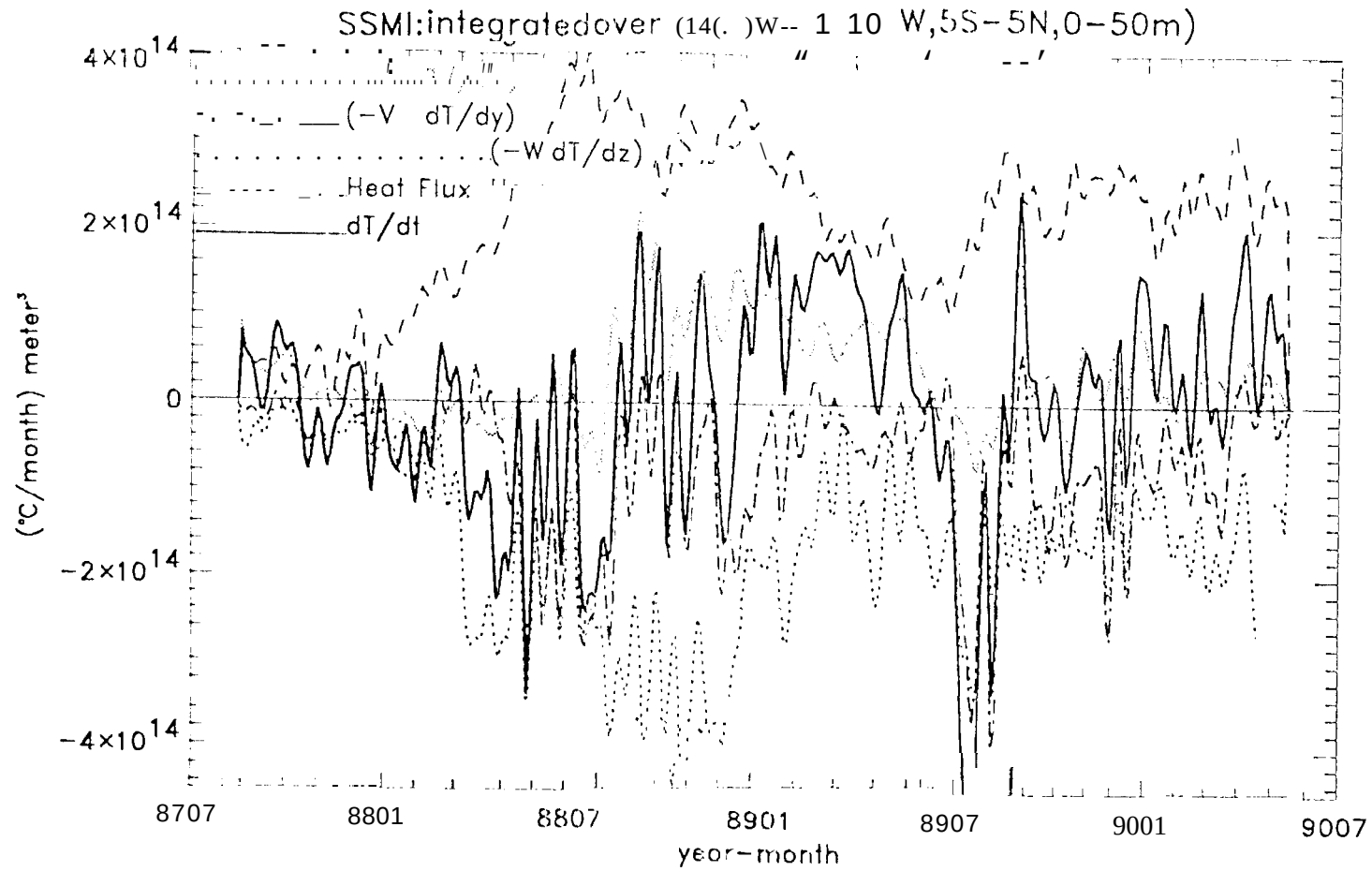

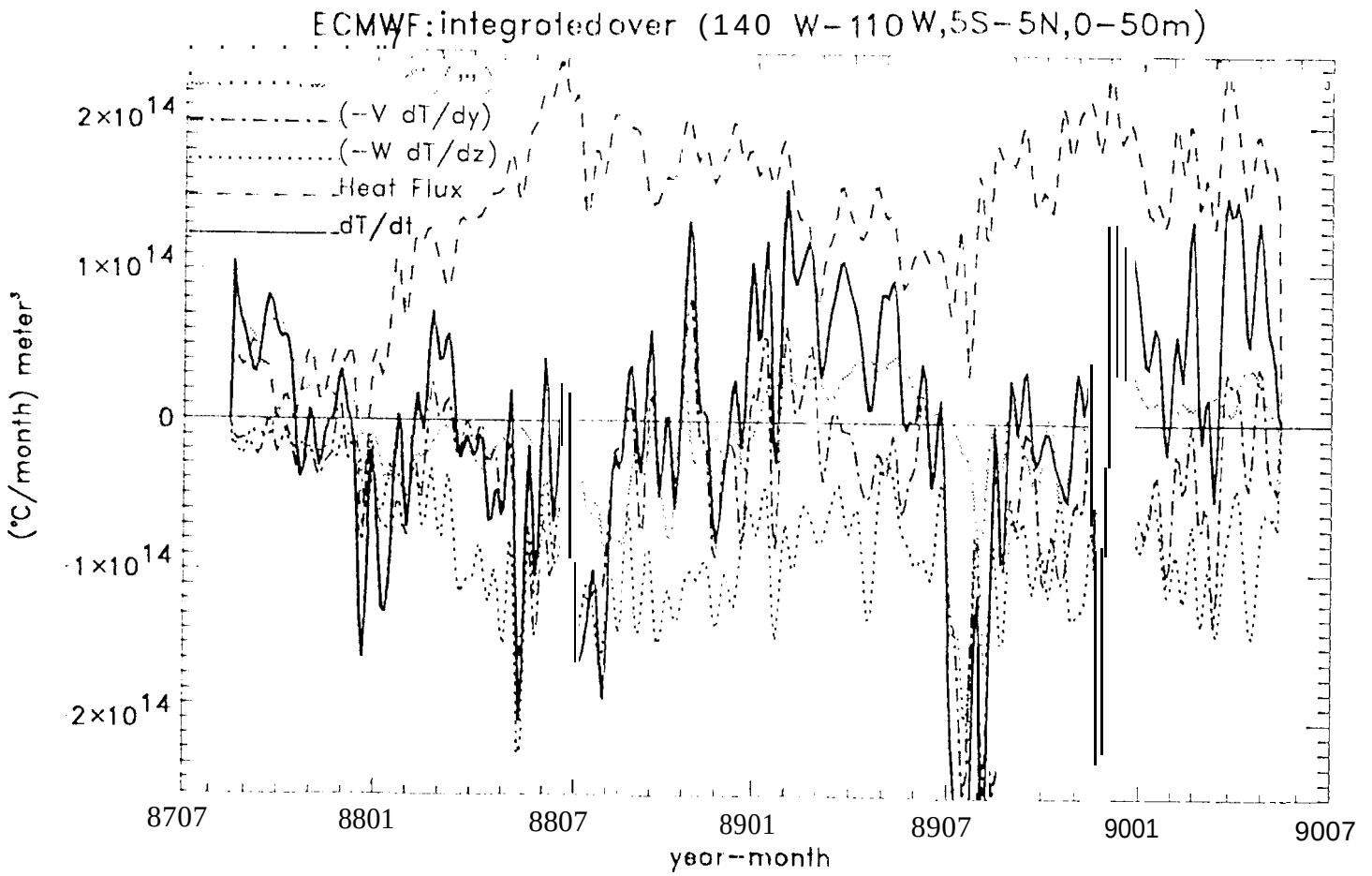

Plotted Oct 17 1995, wqf